THE EFFECT OF POSITION OF PROTRUSIONS ON SLOT JET IMPINGEMENT COOLING OVER A CONCAVE SURFACE

Alankrita Singh[a], C. Balaji[b*], B.V.S.S.S. Prasad[a]

[a] Turbo Machines Laboratory, Department of Mechanical Engineering, Indian Institute of Technology Madras, Chennai- 600036, India
[b] Heat Transfer and Thermal Power Laboratory, Department of Mechanical Engineering, Indian Institute of Technology Madras, Chennai-600036, India

Corresponding author* Email: balaji@iitm.ac.in

Abstract

Numerical simulations are performed to determine the heat transfer characteristics of slot jet impingement of air on a concave surface to emulate the leading edge of a gas turbine vane. Calculations are done with ANSYS Fluent 17.2 using the SST k-ω turbulence model. In order to investigate the effect of protrusions on the heat transfer, a semi-circular protrusion is placed on the concave surface at several positions. After identifying appropriate locations where the heat transfer is a maximum, multiple protrusions are placed at desired locations on the plate. The jet Reynolds number, gap ratio, curvature ratio (d/D) and dimension of plate are varied so as to obtain impingement heat transfer data. The curvature ratio is varied (i) keeping concave diameter (D) fixed and (ii) keeping jet diameter (d) fixed. The Artificial Neural Network is designed to correlate heat transfer according to the parameters mentioned above. This ANN is itself used a surrogate over a large data to predict the optimum locations of the protrusions that maximize the heat transfer from the concave surface through an exhaustive search.

Keywords: Numerical simulations; ANN; Impingement cooling; Protrusion; Concave surface; Slot jet; Heat transfer

NOMENCLATURE

A	cross sectional area of concave surface (m^2)
ANN	Artificial Neural Network
c_p	coefficient of pressure (dimensionless)
D	diameter of curvature of concave surfaces (m)
d/D	curvature ratio (dimensionless)
d	diameter of jet (m)
d_p	diameter of protrusion (m)
G	generation of turbulent kinetic energy ($kg/m\text{-}s^3$)
H	jet to concave surface distance (m)
H/d	gap ratio (dimensionless)
k	thermal conductivity (W/m-K)
LHS	Latin Hypercube Sampling
L	potential core length (m)
MSE	Mean Square Error
Nu	average Nusselt number (Nu = hd/k)
n	total number of output data
Q	amount of heat transferred (w)
q	heat flux (W/m^2)
R	regression coefficient (dimensionless)
RANS	Reynolds Averaged Navier-Stokes
Re	jet Reynolds number ($Re = 4m/(\Pi D_h \mu)$)
SST	Shear Stress Transport
T	temperature (K)
x,y,z	Cartesian co-ordinate
Y	dilation dissipation term ($kg/m^3\text{-}s$)
y+	dimensionless distance (yu_τ/υ)

Greek Symbols

θ	angle between centre of plate to centre of protrusion (˚)
ρ	density (kg/m^3)
μ	dynamic viscosity (kg/m-s)
ω	specific dissipation rate
υ	kinematic viscosity (m^2/s)
δ	momentum thickness (m)
∇	derivative
Δ	difference

Subscripts

ANN	ANN predicted output value
avg	average
i	component along x-direction
j	component along y-direction
k	component along z-direction
u,v,w	component of velocity along x,y,z direction (m/s)
∞	free stream

1. Introduction

Gas turbines are widely used in power generation system and aviation. The inlet temperatures to the turbine must be increased for higher efficiencies. However, this results in the turbine vane/blade getting exposed to higher temperatures. The maximum temperatures are however limited by the safe working temperature of the vane/blades. Whilst film cooling is used to improve heat transfer, convective and impingement cooling techniques are used to remove the heat from the vane/blade surfaces. Impingement cooling is especially used to intensively cool the concave interior leading edge of the vane/blade. Many studies could be found on inclusion of rough structures over target surfaces for augmenting impingement heat transfer over flat surfaces and two pass channels. Khummonghol and Khummonghol [1, 2] declared highest dependence of jet velocity and nozzle size than nozzle height on the performance of an impinging system. During axisymmetric jet impingement on a convex surface, Chung et al. [3] observed increased heat transfer by increasing the pitch of ribs. This was due to increased turbulence intensity due to separation of flow, reattachment and recirculation. Gau and Lee [4, 5] performed slot jet impingement experiments for a triangular flat plate with rectangular and triangular ribs of various pitch-to-height ratios. A larger rib height to slot width ratio of triangular ribs showed lower heat transfer compared to a smooth flat surface. This had been attributed to the formation of air bubbles enclosing the cavity that prevents jet impingement on the wall. Even so, heat transfer by triangular ribs get improved by making the flow turbulent which promotes high momentum exchange and enhances the heat transfer. Higher stagnation Nusselt number was obtained at smaller rib pitch to rib height because of higher circulation in cavity of ribbed wall. Karwa et al. [6] declared that effective efficiency first increases with fluid velocity till it reaches the maximum and then starts decreasing. This was attributed to a remarkable increase in the

pumping power at higher Reynolds number, as the pumping power is a cubic function of the flow velocity. Yan et al. [7] performed experiments on different types of obstacles with several heights in a rectangular channel. They concluded from their investigations that the obstacle height should be optimum (H/d=0.5) in their case for higher heat transfer augmentation. According to them, the obstacle height determines the horseshoe vortex which influences heat transfer. According to Ligrani and Oliveria [8] flow characteristics produced by protrusions, pin fins, ribbed turbulators and dimples decides magnitude of heat transfer. In-line and staggered jet array impingement with different jet exit flow orientation over a ribbed flat plate was studied by Yan et al. [9]. They found both an increase and a decrease in the heat transfer with ribs over a flat surface, compared to a smooth flat surface, depending on the inclination of ribs. Wang and Sunden [10] measured the local Nusselt number variation of square duct with continuous and truncated ribs. They found an overall higher heat transfer augmentation and an attendant increase in the pressure drop by continuous ribs compared to truncated ribs.

Wang et al. [11] found that ribs induce uniformity at higher velocity ratio but rate of augmentation in heat transfer is more at lower velocity ratio. Sharif and Ramirez [12] determined the effect of sand grain roughness heights on turbulent jet impingement over convex surface. They noticed an increase in the heat transfer because of an increase in the turbulence level closer to the convex surface and increase in total convection surface area. Chauhan and Thakur [13] obtained maximum effective efficiency at a jet-to-duct diameter ratio of 0.065 from their developed correlations for an impinging air jet heater. They also confirmed an increase in the efficiency with an increase in the jet flow rate up to certain value. Heat transfer characteristics of secondary hemispherical protrusions in a dimpled cooling channel were studied by Liu et al. [14]. They obtained an increased heat transfer with the inclusion of a secondary protrusion, as

this improves the reattachment and amplifies shedding of the vortex from the dimple. Xie et al. [15] compared heat transfer characteristics of crescent ribs with ribs in a square flow channel. They found higher heat transfer rates with crescent ribs, because of generation of longitudinal vortices which reduces the thickness of the boundary layer. Hwang et al. [16] obtained higher heat transfer and thermal performance at lower Reynolds number, due to larger strength of induced vortices at lower jet velocities. Jang et al. [17] conducted experimental investigations on heat transfer augmentation with dimples and protrusions in a compound ribbed channel. Higher heat transfer was achieved by lower height of protrusion (2.5mm) than with higher semi-spherical protrusions (5mm). Lo and Liu [18] experimentally investigated impingement over half-smooth and half ribbed flat surfaces. They obtained a higher heat transfer by a half rib and half smooth surface compared to fully ribbed plate due to an abrupt change in the surface geometry that favors intense mixing of flow.

Compared to heat transfer studies on ribbed surface/ channels optimization studies on ribbed geometry are scare in literature. Shin et al. [19] reported the requirement of optimization of dimple and channel for better thermal performance. Local heat transfer characteristics on a ribbed channel with different aspect ratio were conducted by Lee et al. [20]. Overall heat transfer was found to be insensitive to channel aspect ratio for 45^0 V-shaped ribs. They suggested optimization for determining the optimal rib configuration and understand the effect of single parameter. Optimization of transverse rib geometry for the highest heat transfer in a circular channel was performed by Kim et al. [21] for an actual turbine cooling passage. Three rib parameters namely- height, width and pitch were considered as design variables whose response surfaces were functions of the friction loss, thermal performance and average Nusselt number ratio. Increasing the rib height promoted the heat transfer, whereas increasing the width degraded

the heat transfer. This occurs due to increase in flow acceleration with the increase of rib width. Kim et al. [22] used the surface response method to optimize a four-variable impinging jet system namely, jet-to-jet spacing, channel height between jet to effusion holes, mass flux of cross flow and main flow temperature. Jin et al. [23] obtained different values of duct-to-rib width for different sets of Reynolds numbers that maximizes the Nusselt number. They also concluded that increasing the rib height causes an improvement in the average Nusselt number but also results in a decrease in the thermo hydraulic performance parameter. Numerical investigations on uniform and non-uniform ribs of a solar duct was investigated by Singh et al. [24]. According to them non-uniform ribs give higher Nusselt number (14-78%) compared to uniform ribs. A multi-objective optimization for delta winglet vortex generator and dimple/protrusion of a solar receiver was proposed by Luo et al. [25]. Dimensionless turbulent kinetic energy and thermal performance were chosen as objective for the optimization whereas, the length, height, angle, depth, spacing of dimple and delta-winglet vortex generator were selected as variables for optimization. Their performance analysis showed that a 72% improvement in thermal performance was possible due to implementation of optimization.

Table 1 summarizes the geometrical dimensions of target and rough geometries considered by various authors. The table shows that the heat transfer depends on various geometrical parameters but generally not all the pertinent parameters have been varied in these studies. It is clear from the above discussion that a rough surface may improve or degrade the amount of heat transfer depending on their geometrical dimensions of the target and the rough geometry and the flow conditions. Furthermore, to the best knowledge of the authors scare are the studies that have considered inclusion of protrusions over a concave surface which represents leading edge of a gas turbine blade and among these are the one by Taslim et al. [29] who considered the inclusion

of protrusion on a concave surface. In their work, a slight improvement in heat transfer (-15% at Re=12500 and 6.6% at Re= 40000) with inclusion of sand roughness, ribs and conical bumps was reported. Even so, the study was confined only to heat transfer characteristics and the fluid flow considerations were left unexplored.

In consideration of the above, the objective and scope of the present study are-

(i) Full numerical simulation of the problem by considering all the geometrical parameters affecting heat transfer characteristics with the help of networking tool in the present study with the help of numerical simulation.

(ii) Development of a surrogate forward model with artificial neural networks (ANNs) with a view to explore the full parametric space.

(iii) Determination of the location of protrusions where higher heat transfer could be achieved by attempting exhaustive search with the surrogate model to replace the time consuming forward model.

2. Computational Methodology

2.1. Computational Model

The physical model of the present study and the associated meshing is shown in Fig. 1. The corresponding boundary conditions of the physical model are given in Table 2. Air at uniform velocity and temperature impinges from a circular jet perpendicularly on an isothermally heated concave surface. The concave surface represents the leading edge of a gas turbine blade. After impinging on the heated concave surface, the air exits to the ambient. The present study considers the following geometrical variants-

(i) smooth semi-circular concave surface

(ii) single protruded semi-circular concave surface at various locations

(iii) smooth concave surface with different curvature ratios (d/D)

(iv) single protruded concave surface with different curvatures

(v) semi-circular concave surface with multiple protrusions

(vi) concave surface with multiple protrusions

2.2 Parameters

The present study investigates the effect of following parameters on the flow and heat transfer characteristics of the slot jet impinging on the concave surface-

(i) gap ratio (H/d)

(ii) curvature ratio (d/D)- (a) fixed D (b) fixed d

(iii) Reynolds number

(iv) location of single protrusion (θ)

(v) location of multiple protrusions

Single protrusions are considered in the simulations by varying their location by a certain angle from the preceding simulation. In all, calculations are done for 60 cases for the single protrusion variant of the problem. Thereafter; multiple protrusions are considered, based on outcomes of the single protrusion data. The overall computational set is given in Table 3.

2.3. Computational Methods

Due to non-variation of temperature along the axial direction and flow symmetry in slot jet impingement problem, two-dimensional simulations are employed [30]. It is assumed that the fluid flow is steady and incompressible. Effects of buoyancy and viscous dissipation are ignored. With the second order upwind discretization scheme, the governing equations of continuity, momentum and energy with the SST k-ω turbulence model are solved by pressure-based solver.

The governing equations are -

Equation of continuity:

$$\nabla.(\rho u) = 0 \tag{1}$$

Equation of momentum:

$$(u.\nabla)u - \frac{1}{\rho}\nabla p + \upsilon\nabla^2 u = 0 \tag{2}$$

Equation of energy:

$$\rho c_p(u.\nabla T) - k\nabla^2 T = 0 \tag{3}$$

Equation of turbulent kinetic energy (k):

$$\frac{\partial}{\partial x_i}(\rho k u_i) = \frac{\partial}{\partial x_j}\left(\Gamma_k \frac{\partial k}{\partial x_j}\right) + \overline{G_k} - Y_k + \delta_k \tag{4}$$

Equation of specific dissipation:

$$\frac{\partial}{\partial x_i}(\rho w u_i) = \frac{\partial}{\partial x_j}\left(\Gamma_w \frac{\partial w}{\partial x_j}\right) + \overline{G_w} - Y_w + D_w + \delta_w \tag{5}$$

where, $\Gamma_k = \mu + \frac{\mu_t}{\sigma_u}$, $\quad \Gamma_w = \mu + \frac{\mu_t}{\sigma_w}$

Semi-Implicit Method for Pressure-Linked Equation (SIMPLE) algorithm is used for pressure-velocity coupling. If the sum of normalized residuals drops below 10^{-5} for continuity, momentum and turbulence equation and 10^{-7} for energy equation, the solution is assumed to be converged.

2.4. Validation

Since no heat transfer data is available on protruded concave surfaces, the present computational methodology is validated for a smooth concave surface. Thereafter, the same smooth surface is

modified by adding protrusions. Experimental results of Choi et al. [30] for a Reynolds number of 4740 and a gap ratio of 4 are used for the purpose of validation. The results of this exercise are shown in Fig. 2(a). Different turbulence models were employed to solve the problem and among these SST k-ω model predicted better with higher convergence of 10^{-5} and better agreement with the results of Choi et al. [30]. This occurs so because the SST k-ω model combines the standard k-ε model with the standard k-ω model. In the SST k-ω model, the standard k-ε model is used away from the wall and the standard k-ω model near the wall and discrepancies that occur near the wall due to not so perfect representation of turbulence in the k-ε model is mitigated to a large extent. Average Nusselt number data are also validated with the correlation provided by Sharif and Mothe [31] and the result of the comparison are shown in Fig 2(b).

2.5. Grid Independency Test

A grid independence study with different sizes of mesh is carried out for grid dependency test and the results of this exercise are shown in Fig. 3. Following the grid independence test, computational grids with 175000 and 190000 nodes are chosen for the smooth and protruded concave surfaces respectively.

3. Results and Discussion

Background of the study

Calculations are done for both smooth and multiple protruded (N=21) concave surfaces at a fixed Reynolds number of 4060 and a gap ratio of 3 and the results are shown in Fig. 4. Following these, calculations are done for two different diameters of protrusion (d_p= 3mm and 5mm). It is expected that all sets of multiple protruded surface would enhance heat transfer due to increase in available surface area but the reverse happened. However, the average Nusselt number alone

does not indicate that protrusions should not be implemented for augmentation of heat transfer over concave surfaces. When local Nusselt numbers are measured along the smooth and multiple protruded surfaces, it is seen that although overall protrusions fail to enhance heat transfer they locally do improve the rate of heat transfer. This motivates one to determine the location for allocation of protrusion for successful augmentation of overall heat transfer. Therefore, the present study is devoted to study of location of protrusion over a curved surface.

3.1. Effect of heat transfer with location of single protrusion

Single protrusions of different diameters have been considered at various location of concave surface from 0°-80° with continuous interval of 10°. As seen from Fig. 5, most of the protrusions are helpful in the range of 40°-70°. The difference in rate of increase of average Nusselt number and total amount of heat transferred simply indicate that protrusion area is responsible for enhancement of heat transfer along with the heat transfer coefficient. Protrusions near the center of plate fail to enhance heat transfer because of swaying of the jet from the curved wall. The reasons could be explained from the velocity contours shown in Fig.6. From the figure, it is seen that high convective region is concentrated near the stagnation point. If protrusions are placed in this region, they cause a negative effect on impingement heat transfer because the jet loses its impingement effect. In other words, the strength of the jet reduces. Protrusions placed just below the jet bifurcates jet stream in random directions without hitting the nearest curved wall and thereby the strength of the jet reduces. Apart from bifurcation of jet, a recirculation is formed on the other side of protrusion facing the end of the curved surface. These recirculating vortices are responsible for the decrease in the heat transfer at the notches of the protrusion. For $\theta = 0°$, this recirculating vortex is absent. At higher angles ($\theta \geq 30°$) the jet starts accelerating which results in augmentation of the heat transfer. Results for this are shown in Fig. 7. The secondary peaks of

Nusselt number are seen at locations of protrusion which change the amount of heat transfer compared to corresponding smooth surface.

3.2. Effect of curvature ratio (d/D)

The effect of curvature ratio can be studied by varying the diameter of jet for a fixed diameter of curved surface or by varying the diameter of the concave surface at fixed diameter of jet. Fig. 8 shows the local Nusselt number variation for various sets of diameter of jet (d=2mm and 2.5mm) and diameter of concave surface (D= 160mm and 200mm) corresponding to a fixed curvature ratio (d/D) of 0.0125 at fixed flow condition (Re=4060) and gap ratio. It is inferred from the figure that there is 10 and 8.6% variation in average and stagnation Nusselt number respectively between the two dimensional sets of jet and concave surface. This shows that curvature ratio should not be non-dimensionalized for characterizing the curvature effect on jet impingement heat transfer.

3.3. Fixed diameter of curved surface

Fig. 9 shows the local Nusselt number behavior for two different diameters of jet, namely d=2 and 3.25mm during slot jet impingement cooling over a concave surface (D=160mm, H/d=3 and Re=4060). It can be seen from the plot that a smaller jet possess a higher stagnation Nusselt number but lower average Nusselt number. This can be explained with variation in the potential core length with change in the dimension of jet. Fig. 10 and 11 clearly shows that the smaller dimension of jet possesses lower jet-to-plate distance ($H_1<H_2$ in Fig.10) and lower potential core length ($L_1<L_2$ in Fig. 11) compared to a larger diameter jet. Because of lower jet-to-plate distance, some part of the potential core is capable of reaching the stagnation region which

results in a higher stagnation Nusselt number for a smaller jet. For both the smaller and larger jets, the Nusselt number continuously reduces along the downstream direction.

Fig. 12(a) shows a plot of the average Nusselt number for two different diameter of jet, namely d=2 and 3.25mm at various locations of the protrusion for a fixed Reynolds number of 4060 and gap ratio of 3. From the figure it is evident that the trend in the variation of heat transfer remains the same for both jets. A wider jet (d= 3.25mm) gives a larger average Nusselt number compared to a smaller jet dimension (d=2mm) for a given Reynolds number. This is attributed to more dependence of Nusselt number on the flow rate compared to jet velocity or Reynolds number according to following equation-

$$Re = \frac{v\rho d}{\mu} = \frac{4m}{\pi d\mu} \tag{6}$$

Similar observations have also been made by Gau and Chung [32]. The larger diameter of jet results in pre-vortex initialization in the mixing region of the jet. This is confirmed with larger jet-to-plate distance and larger momentum transport.

Notwithstanding the above discussion, if one looks at the amount of heat energy exiting from the domain of interest (Fig. 12(b)) it is noticed that the Nusselt number being a non-dimensional number is misleading. A comparison of actual heat transfer results with the amount of heat being released after the impingement effect may throw more light on the physics of the problem. Contrary to average Nusselt number results, a smaller diameter of jet possesses higher turbulence intensity which contributes to augmentation in the heat transfer at lower diameter of jet (Fig. 13(a)). This indicates that the jet turbulent intensity dominates the jet velocity in the heat transfer process. The turbulence intensity starts increasing gradually as the jet departs away from the jet exit and it suddenly drops as soon as the jet hits any protrusion/ concave surface. Since the

turbulence intensity increases with the increase of distance therefore, higher turbulence intensity is observed for smooth and all protruded cases except central protrusion ($\theta = 0^{o}$). This is because of a reduction in jet to target distance.

As already discussed it is noticed that for any dimension of jet the protrusions are beneficial for increasing heat transfer in the range of $40^{o} \leq \theta \leq 80^{o}$. Fig. 13(b) shows similar results.

3.4. Fixed diameter of jet

Fig. 14(a) and (b) show that an increase in the diameter of concave surface reduces average Nusselt number and heat transfer. In other words, the heat transfer decreases as the surface approaches planar limit. The increase in heat transfer for a semicircular surface (D=160mm) is accompanied by increase in the Görtler number with an increase in the curvature ratio of the concave surface. The Görtler number signifies relation between destabilising centrifugal force and inertial forces with the stabilising viscous force. It is given by-

$$G_{\theta} = \frac{U_{\infty}\delta}{\vartheta}\sqrt{2\delta/D} \tag{7}$$

Where the Blasius momentum thickness is represented as-

$$\delta = \sqrt{\frac{\vartheta x}{U_{\infty}}} \tag{8}$$

As seen from Fig.15, the Görtler number is larger for semicircular concave surface compared to higher curvature (D=260mm) surface along the streamwise direction. The higher Görtler number results in augmentation in heat transfer for smaller curvature surface.

3.5. Effect of the gap ratio

Fig. 16(a) and (b) show the effect of gap ratio on the average Nusselt number and heat transfer respectively. The figure clearly shows an increasing trend with the gap ratio becoming more prominent if the protrusion is placed $30^0 \leq \theta \leq 80^0$. This is attributed to larger pressure gradient between wall jet region and flow region for $\theta \geq 30^0$. Highest overall heat transfer is achieved for a gap ratio of 3. A larger value of gap ratio (such as H/d=9) has larger pressure gradient and this, in turn, increases the boundary layer thickness and hence reduces the heat transfer.

3.6. Effect of the diameter of the protrusion

Fig. 17(a) and (b) show the effect of diameter of the protrusion on the average Nusselt number and overall heat transfer respectively. From the figure, it is noticed that smaller protrusions (d_p=2mm) perform better than larger ones (d_p =3 and 5mm) in terms of Nusselt number. However, in terms of heat transfer the larger protrusions seem to perform better. This indicates the lower contribution of heat transfer coefficient on the protruded concave surface with larger dimension of protrusions. For some of the location of protrusions (θ =0°, 10° and 20°), the heat transfer value decreases with an increase in the diameter of protrusion (d_p=5mm) which shows that an increase in the surface area does not necessarily indicates an increase in amount of the heat transfer. Further, corresponding to $\theta = 20^0$ the smaller diameter protrusion (d_p=2mm) shows exceptionally high average Nusselt number and heat transfer. This could be because of certain favorable modifications in the jet flow structure which helps in augmentation of heat transfer.

3.7. Multiple Protrusions

From the preceding discussion, it is evident that protrusions are helpful in heat transfer augmentation only if they are included at desired locations. Test and trials of many multiple and single protrusions were carried out for several range of gap ratios, curvature ratio, and dimension

and location of protrusion. The data set of all parameters is generated using Latin Hypercube Sampling (LHS) [33]. The upper and lower bounds considered for LHS are given in Table 4. Since, the product of velocity of jet and diameter of jet remains constant at fixed Reynolds number therefore, only jet diameter is considered as input variable among the two. The corresponding velocity of jet is calculated using the continuity equation. Between 1 and 16 protrusions are allocated on a half symmetric concave surface (θ = 0°, 10°, 20°, 25°, 30°, 35°, 40°, 45°, 50°, 55°, 60°, 65°, 70°, 75°, 80° and 85°). For ease of sample generation these 16 angular positions are converted to one variable by using binary bit 0 and 1. The 16 bit binary string thus generated is converted to its decimal equivalent. In this way 16 variables of position of protrusions (θ) are made as one variable for LHS. Following this there can be 2^{16} configurations of allocation of protrusions. Subsequently, the lower bound of position variable becomes 1 corresponding to single protrusion and upper bound takes a value of 65535 denoting protrusions present at all 16 positions. For better understanding Table 5 shows a few configurations along with their binary equivalent. A total 10500 samples are generated using the LHS.

Among 10500 data sets, random 455 samples are selected and simulated to obtain output data in terms of amount of heat being exited from the domain of interest. Similar to what is observed for the single protrusion case, it is seen that multiple protrusions are beneficial in heat transfer augmentation if they are placed away from stagnation point ($\theta \geq 30°$). A new term enhancement ratio is used to calculate the rate of augmentation in heat transfer. This is defined as ratio of amount of heat transferred by protruded concave surface to its corresponding smooth configuration. However, multiple protrusions also lead to increase in surface area.

3.8. Artificial Neural Network

In order to save computation time the data output of remaining samples are determined using Artificial Neural Network. Fig. 18 shows the typical structure of single layer ANN model used in the present study. In this model multiple locations of protrusions is considered as single variable by converting every set of locations into decimal equivalent. Since an increase in the number of hidden layer did not bring any change in the value of output therefore single hidden layer is chosen for the present neural network study. The output layer has one node which represents the amount of heat exiting the domain after impingement.

3.9. Optimization of heat transfer

The optimization problem under consideration is the maximization of the heat transfer rate, Q subject to certain constraints. These can be represented mathematically as follow-

$$Maximize\ Q = f\left(D, d, d_p, \frac{H}{d}, \theta\right) \tag{9}$$

Subject to:

$$160 \leq D \leq 260 \tag{10}$$

$$2 \leq d \leq 5 \tag{11}$$

$$1.5 \leq d_p \leq 3.25 \tag{12}$$

$$3 \leq \frac{H}{d} \leq 9 \tag{13}$$

$$0° \leq \theta \leq 85° \tag{14}$$

where,

D: diameter of the concave surface

d: diameter of the jet

d_p: diameter of the protrusion

H/d: gap ratio

θ: angle between the centre of the plate to centre of the protrusion

It is instructive to mention that the function 'f' is not explicitly known in this formidable, non-linear problem. The function 'f' is replaced by a surrogate ANN model, which is then maximized by exhaustively exploring the parameter space. The exhausting search is affordable by the ANN that returns 'f' for a given set of (D, d, d_p, H/d, θ) in a fraction of the time taken by full numerical simulations. Prior to ANN modeling multiple simulations were run considering all the five input variables. Before training of data sets 40% of the simulated data sets are kept aside for the purpose of validation of developed neural network model. By trial and error method, the architecture of ANN model is decided. The Levenberg-Marquardt is used as the training algorithm. The chosen model has 5-3-1 structure which constitutes 5 neurons in the input layer, 3 in the hidden layer and 1 neuron in the output layer which corresponds to amount of heat transferred. Among 455 samples of input data, 80% of the data is allocated for training and 10% for testing and 10% for validation. The ANN model is chosen for a function which gives highest R value and least MSE, as presented in Table 6. High order of MSE is obtained because of extreme outliers in the input variables. Fig.19 shows a regression plots corresponding to the training, testing and validation of the neural network and configures the adequacy of the ANN.

For the purpose of validation of ANN data some of the results are tested by running simulations at same parameter and boundary condition of input data sets. The corresponding parity plot is shown in Fig. 20. The figure confirms the adequacy of the ANN to predict the impingement heat

transfer with an uncertainty of ±1.5%. Using this network an exhaustive search is carried out. The exhaustive search results in the following configuration that gives the maximum heat transfer at Reynolds number of 4060-

$$\left\{\begin{matrix} D = 220mm \\ d = 1.5mm \\ d_p = 5mm \\ \frac{H}{d} = 4 \\ \theta = \begin{pmatrix} 40° \\ 45° \\ 50° \\ 55° \\ 60° \\ 65° \\ 70° \\ 75° \\ 80° \end{pmatrix} \end{matrix}\right\} \text{with Q} = \ 1309.22\text{W} \qquad (15)$$

This is a key result of this study. Full numerical simulations are then done for the best configuration and the results have been compared with those for the no protrusion case. The enhancement ratio of the best configuration is 1.08. The ratio of the surface area of the protruded to the smooth concave surface is 1.2. This indicates that major contribution of heat transfer enhancement of this configuration is due to change in surface area. However, again it is to be noted that increase in surface area does not always signify increase in amount of heat transfer.

For gaining confidence on the optimal solution trough the ANN a sensitivity study of the best configuration model has been carried out. The input variable of the best configuration model are perturbed and these perturbed input data are used to determine the amount of heat transferred. Results of this exercise are given in Table 7. It is noticed from the table that a slight change in value of input variables bring large change in heat transfer. Even so, in no case is the heat transfer more than that obtained for the optimum configuration. Hence, it is confirmed that the

configurations are sensitive to input variables and among 10500 sets of configurations the obtained best configuration model (highlighted in Table 7) gives the highest heat transfer and enhancement factor.

4. CONCLUSIONS

Slot jet impingement cooling over various configurations of protruded concave surface has been numerically studied in the present paper. Before moving to multiple protrusions, the effect of single protrusion for various curvature of concave surface was investigated. The samples for various configurations of protruded concave surface were generated using Latin Hypercube Sampling. Thereafter, ANN as a predictive tool is used to find out the best configuration for highest amount of heat transfer. An increase in surface area with inclusion of protrusion does not necessarily indicate an increase of heat transfer. Following are the major conclusions drawn from the study-

- Inclusion of protrusion at and near the stagnation region ($\theta \leq 30^{o}$) results in a decrease in heat transfer because of a decrement in the jet strength, at high convective region.
- High potential core is observed for larger width of jet and turbulence intensity increases as the jet moves away from its exit.
- For a fixed diameter of concave surface, a smaller jet possesses high turbulence intensity contributing to augmentation in heat transfer.
- High curvature surface with a fixed dimension of jet possesses greater momentum thickness and hence lesser heat transfer ability.

- ANN is a powerful tool to not only predict impingement heat transfer characteristics by considering multiple parameters but also to determine the optimum configuration from many thousands of candidate solutions.
- A maximum increase of 8% in the heat transfer is obtained by the best configuration constituting of multiple protrusions. This is not insignificant in the case of applications concerning gas turbine blade cooling.

References

1. D. Khummongkol, P. Khummongkol, "Heat transfer between an impinging air jet and an impinged water surface." Energy, 23 (1998), pp. 239-245.
2. D. Khummongkol, P. Khummongkol, "Theoretical analysis of dust removal from gas impinging on a confined liquid surface." Energy, 19 (1994), pp. 817-824.
3. Y.S. Chung, D.H. Lee, J.S. Lee, "Heat transfer characteristics of an axisymmetric jet impinging on the rib-roughened convex surface." International Journal of Heat and Mass Transfer, 42 (1999), pp. 2101-2110.
4. C. Gau, C.C. Lee, "Impingement cooling flow structure and heat transfer along triangular rib roughened walls." International Journal of Heat and Mass Transfer, 35 (1992), pp. 3009-3020.
5. C. Gau, I.C. Lee, "Flow and impingement cooling heat transfer along triangular rib-roughened walls." International Journal of Heat and Mass Transfer, 43 (2000), pp. 4405-4418.
6. R. Karwa, S.C. Solanki, J.S. Saini, "Thermo-hydraulic performance of solar air heaters having integral chamfered rib roughness on absorber plates." Energy, 26 (2001), pp. 161-176.
7. W.M Yan, R.C. Hsieh, C.Y. Soong, "Experimental study of surface-mounted obstacle effects on heat transfer enhancement by using liquid crystal thermograph." ASME Journal of Heat Transfer, 124 (2002), pp. 762-769.
8. P. M. Ligrani, M.M. Oliveria, "Comparison of heat transfer augmentation techniques." AIAA Journal, 41 (2003), pp. 337-362.
9. W.M. Yan, H.C. Liu, C.Y. oong, W-J Yang, "Experimental study of impinging heat transfer along rib-roughened walls by using transient liquid crystal technique." International Journal of Heat and Mass Transfer, 48 (2005), pp. 2420-2428.
10. L. Wang, B. Sunden, "Experimental investigation of local heat transfer in a square duct with continuous and truncated ribs." Experimental Heat Transfer, 118 (2005), pp. 179-197.

11. C. Wang, B. Sunden, A. Borg, H. Abrahamsson, “Control of jet impingement heat transfer in crossflow by using a rib.” International Journal of Heat and Mass Transfer, 54 (2011), pp. 4157-4166.
12. M.A.R. Sharif, N.M. Ramirez, “Surface roughness effects on the heat transfer due to turbulent round jet impingement on convex hemispherical surfaces.” Applied Thermal Engineering, 51 (2013), pp. 1026-1037.
13. R. Chauhan, N.S. Thakur, “Investigation of the thermohydraulic performance of impinging jet solar air heater.” Energy, 68 (2014), pp. 255-261.
14. J. Liu, Y. Song, G. Xie, B. Sunden, “Numerical modeling flow and heat transfer in dimpled cooling channels with secondary hemispherical protrusions.” Energy, 79 (2015), pp. 1-19.
15. G. Xie, X. Liu, H. Yan, J. Qin, “Turbulent flow characteristics and heat transfer enhancement in a square channel with various crescent ribs on one wall.” International Journal of Heat and Mass Transfer, 115 (2017), pp. 283-295.
16. S.D. Hwang, H.G. Kwon, H.H. Cho, “Local heat transfer and thermal performance on periodically dimple-protrusion patterned walls for compact heat exchangers.” Energy, 35 (2010), pp. 5357-5364.
17. H.N. Jang, J.S. Park, J.S. Kwak, “Experimental study on heat transfer characteristics in a ribbed channel with dimples, semi-spherical protrusions, or oval protrusions.” Applied Thermal Engineering, 131 (2018), pp. 734-742.
18. Y.H. Lo, Y-H Liu, “Heat transfer of impinging jet arrays onto half-smooth, half-rough target surfaces.” Applied Thermal Engineering, 128 (2018), pp. 79-91.
19. S. Shin, K.S. Lee, S.D. Park, J.S. Kwak, “Measurement of the heat transfer coefficient in the dimpled channel; effects of dimple arrangement and channel height.” Journal of Mechanical Science and Technology, 23 (2009), pp. 624-630.
20. D.H. Lee, D.H. Rhee, K.M. Kim, H.H. Cho, H.K. Moon, “Detailed measurement of heat /mass transfer with continuous and multiple V-shaped ribs in rectangular channel.” Energy, 34 (2009), pp. 1770-1778.
21. K.M. Kim, B.S. Kim, D.H. Lee, H. Moon, H.H. Cho, “Optimal design of transverse ribs in tubes for thermal performance enhancement.” Energy, 35 (2010), pp. 2400-2406.
22. K.M. Kim, H. Moon, J.S. Park, H.H. Cho, “Optimal design of impinging jets in an impingement/ effusion cooling system.” Energy, 66 (2014), 839-848.
23. D. Jin, M. Zhang, P. Wang, S. Xu, “Numerical investigation of heat transfer and fluid flow in a solar air heater duct with multi V-shaped ribs on the absorber plate.” Energy, 89 (2015), pp. 178-190.
24. S. Singh, B. Singh, V.S. Hans, R.S. Gill, “CFD (Computational Fluid Dynamics) investigation on Nusselt number and friction factor of solar air heater duct roughened with non-uniform cross-section transverse rib.” Energy, 84 (2015), pp. 509-517.

25. L. Luo, W. Du, S. Wang, L. Wang, B. Sunden, X. Zhang, “Multi-objective optimization of a solar receiver considering both the dimple/ protrusion depth and delta-winglet vortex generators.” Energy, 137 (2017), pp. 1-19.
26. Y-J Hong, S.S. Hsieh, “Heat transfer and friction factor measurement in ducts with staggered and inline ribs.” ASME Journal of Heat Transfer, 115 (1993), pp. 58-65.
27. J.C. Han, J.S. Park, “Developing heat transfer in rectangular channels with rib turbulators.” International Journal of Heat and Mass Transfer, 31 (1988), pp. 183-195.
28. J.C. Han, S. Ou, J.S. Park, C.K. Lei, “Augmented heat transfer in rectangular channels of narrow aspect ratios with rib turbulators.” International Journal of Heat and Mass Transfer, 32 (1989), pp. 1619-1630.
29. M.E. Taslim, L. Setayeshgar, S.D. Spring, “An experimental evaluation of advanced leading edge impingement cooling concepts.” Journal of Turbomachinery, 123 (2001), pp. 147-153.
30. M. Choi, H.S. Yoo, G. Yang, J.S. Lee, D.K. Sohn, “Measurement of impinging jet flow and heat transfer on a semi-circular concave surface.” International Journal of Heat and Mass Transfer, 43 (2000), pp. 1811-1822.
31. M.A.R. Sharif, K.K. Mothe, “Parametric study of turbulent slot jet impingement heat transfer from concave cylindrical surfaces.” International Journal of Thermal Sciences, 49 (2010), pp. 428-442.
32. C. Gau, C.M. Chung, “Surface curvature effect on slot-air-jet impingement cooling flow and heat transfer process.” ASME Journal of Heat Transfer, 113 (1991), pp. 858-864.
33. J. Park, K.S. Lee, M.S. Kim, D. Jung, “Numerical analysis of a dual-fueled CI (compression ignition) engine using Latin Hypercube sampling and multi-objective Pareto optimization.” Energy, 70 (2014), pp. 278-287.

LIST OF TABLES

Table 1. Summary of previous research on rough surfaces

Authors	Target surface	Type of roughness	Outcome
[4]	flat	rectangular, triangular ribs	rib pitch to height= 0.25 performs better than 0.5, jet dia to height of rib= 1.17-6.67
[7]	flat	circular square rhombus ribs	rib height to depth ratio= 0.5
[10]	square duct	rectangular	rib height to depth ratio= 0.15, pitch to height ratio= 12
[15]	square channel	crescent ribs	best overall performance at rib to channel width= 0.4
[17]	ribbed channel	semi-spherical protrusion	height of rib to width of channel
[21]	circular channel	rectangular ribs	rib pitch to height ratio= 5.31, rib height to width ratio= 0.1-0.125 for real gas turbine (optimum): rib width to height= 2.753, rib pitch to width= 9.694
[23]	duct	multi V-shaped ribs	duct width to rib width= 6.3
[26]	square, rectangular channel	inline, staggered ribs	rib height to width ratio= 0.19, 0.143, rib pitch to height ratio= 5.31
[27]	square duct	angular ribs	rib height to width ratio= 0.047, 0.078
[28]	rectangular duct	angular ribs	rib height to width ratio= 0.19, 0.143

Table 2: Details of boundary conditions

S.N.	Location	Variables	Value
1	Velocity inlet	Temperature Reynolds number	300K 4060
2	Target concave plate	Constant temperature	335K
3	Slot jet wall	Heat flow	Insulation
4	Outlet	Constant pressure	Pressure outlet

Table 3. Computational matrix for the cases investigated in the present study

Geometry	H/d	Re	Location of protrusion	D	d	No. of cases
smooth	3, 5, 9	4060	-	160,260	2, 3.25	6
single protrusion	3, 5, 9	4060	0°-80°	160, 260	2, 3.25	60
multiple protrusions	3	4060	0°-80°	160-260	1.5-3.25	10500

Table 4. Lower and upper bounds of variables considered for Latin Hypercube Sampling

Variables	Lower Bound	Upper Bound
D	160mm	260mm
d_p	2mm	5mm
d	1.5mm	3.25mm
H/d	3	9
θ	0^0	85°

Table 5. Binary equivalent of sample configuration numbers designating location of protrusion

Configuration number	Binary Equivalents	Location of protrusion (θ)
496	0000111110000000	±(30°-35°-40°-45°-50°)
21824	0000001010101010	±(40°-50°-60°-70°-80°)
21846	0110101010101010	±(10°-20°-30°-40°-50°-60°-70°-80°)
32768	0000000000000001	±85°

Table 6. Results of the neuron independence study

No. of neurons	Training		Testing	
	MSE	R	MSE	R
2	53	0.99970	897.48	0.96076
3	**24**	**0.99978**	**500.08**	**0.98983**
4	208.13	0.98943	1007.18	0.97652
5	60	0.99970	654.70	0.97944

Table 7. Effect of perturbation in values of decision variables from their optimum on the heat transfer rate (Q) and enhancement ratio of the concave surface

Input Variables						Heat transfer rate	Enhancement
D (mm)	dp (mm)	d (mm)	v (m/s)	H/d	θ (θ_1,Δθ,θ_2)	Q (W)	Ratio
220	**5**	**1.5**	**40**	**4**	**40°, 5, 80°**	**1309.2**	**1.08**
220	5	1.5	40	3	40°, 5, 80°	1278.4	1.05
220	6	1.5	40	4	40°, 5, 80°	1263.7	1.04
220	5	1.5	40	4	40°, 5, 80°	1274.8	1.05
220	5	1.5	40	4	35°, 5, 80°	1258	1.04
200	5	1.5	40	4	40°, 5, 80°	1267.3	1.05
220	5	2	30	4	40°, 5, 80°	1102.2	1.05
220	4	1.5	40	4	40°, 5, 80°	1257.6	1.04
200	4	2	30	5	40°, 5, 80°	1098.5	1.05

LIST OF FIGURES

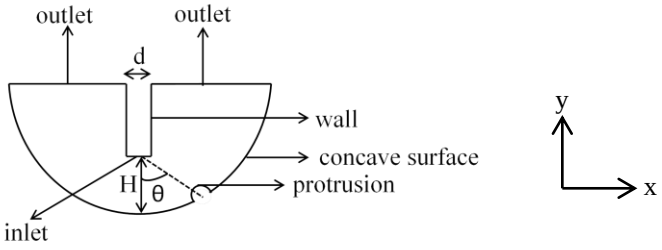

(a) Computational model

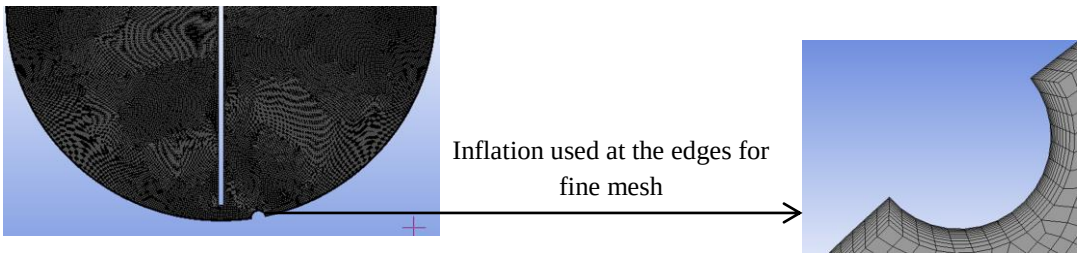

(b) Meshing used in the present study

Fig. 1. Computational model and meshing employed in the present study

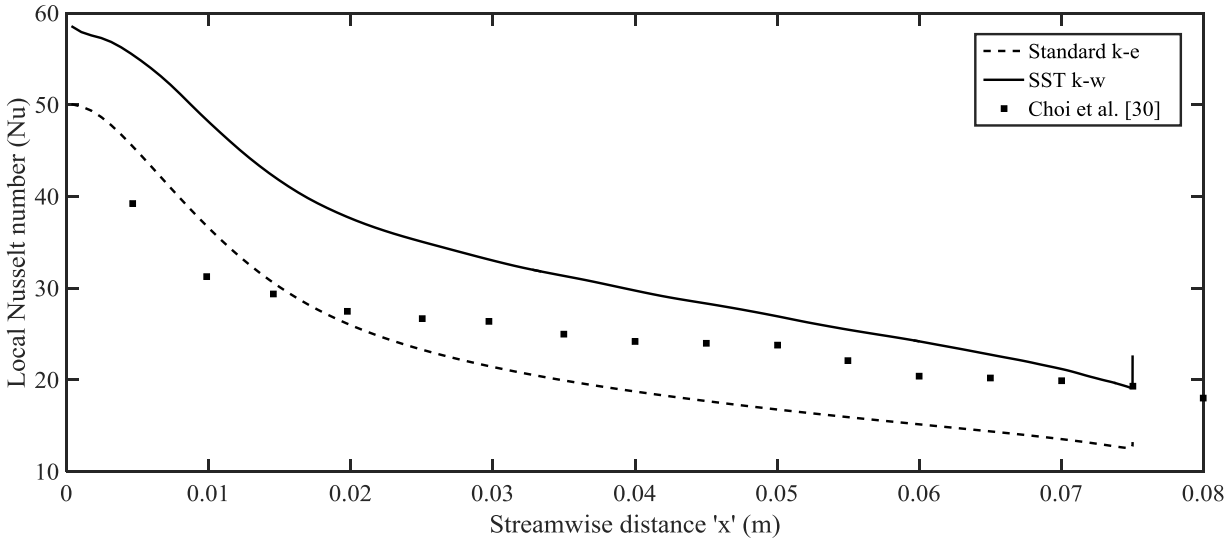

(a) Validation with experimental results from literature [30]

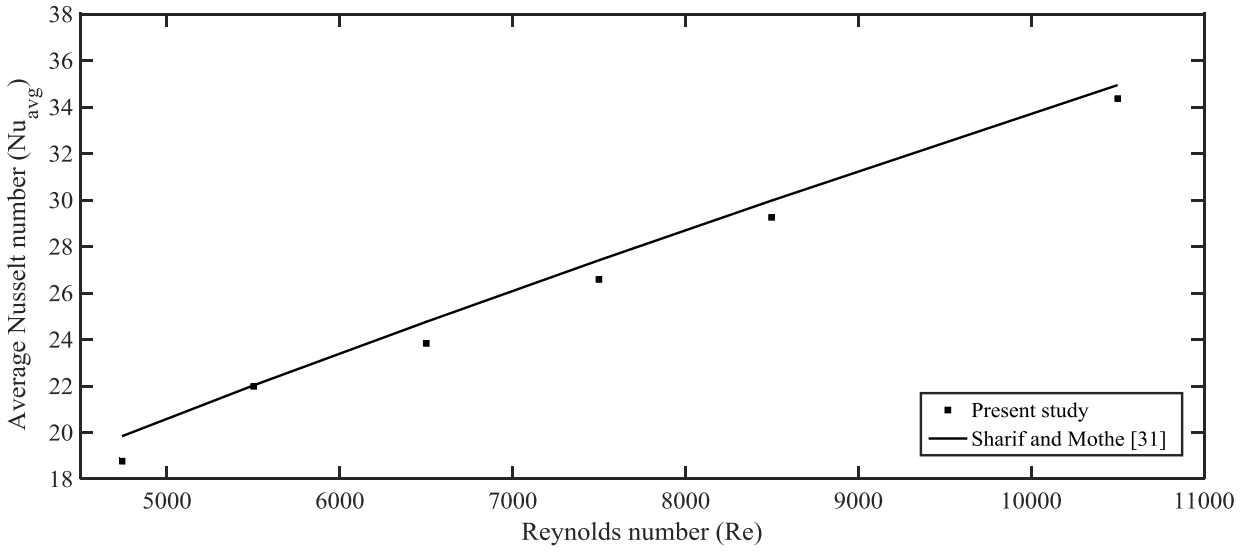

(b) Validation with correlation from literature [31]

Fig. 2. Validation of the numerical methodology employed in the present study

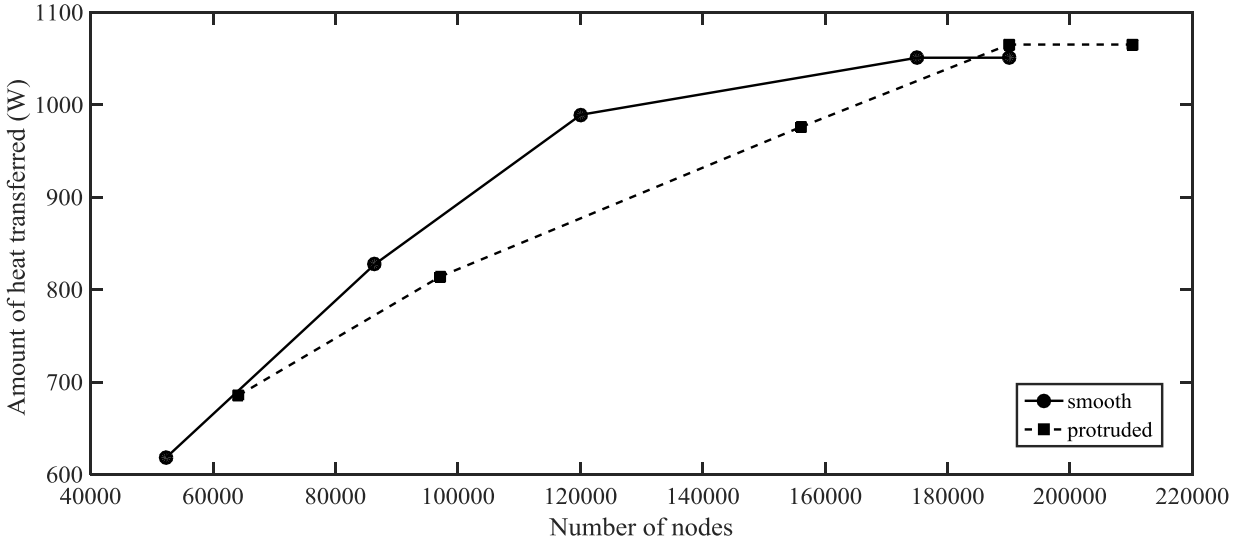

Fig. 3: Results of the grid independence test

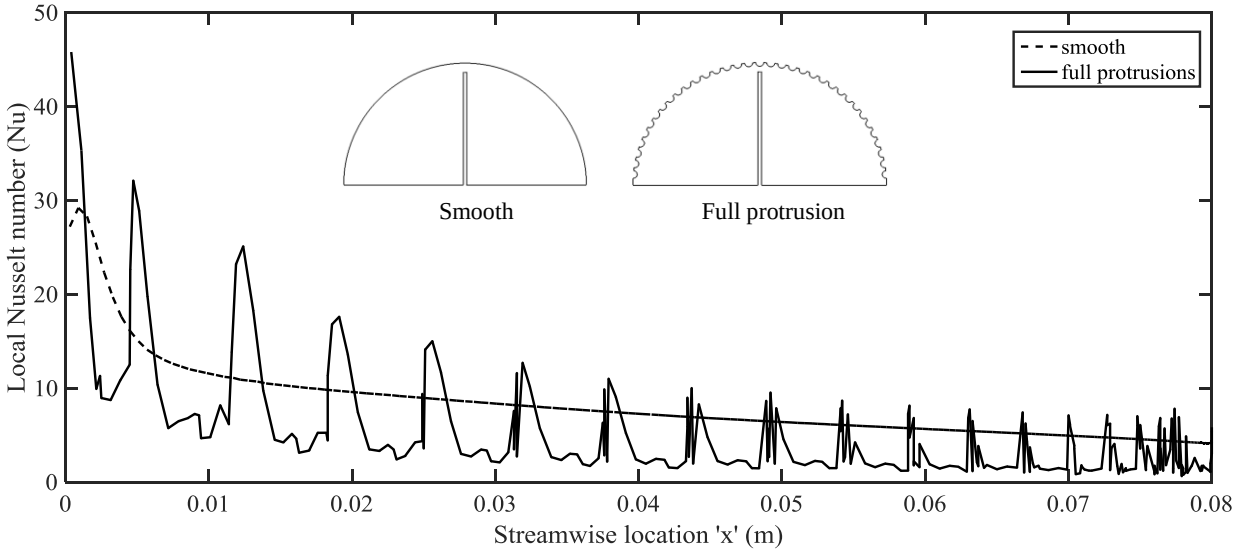

Fig. 4. Distribution of Nusselt number for smooth and protruded surfaces

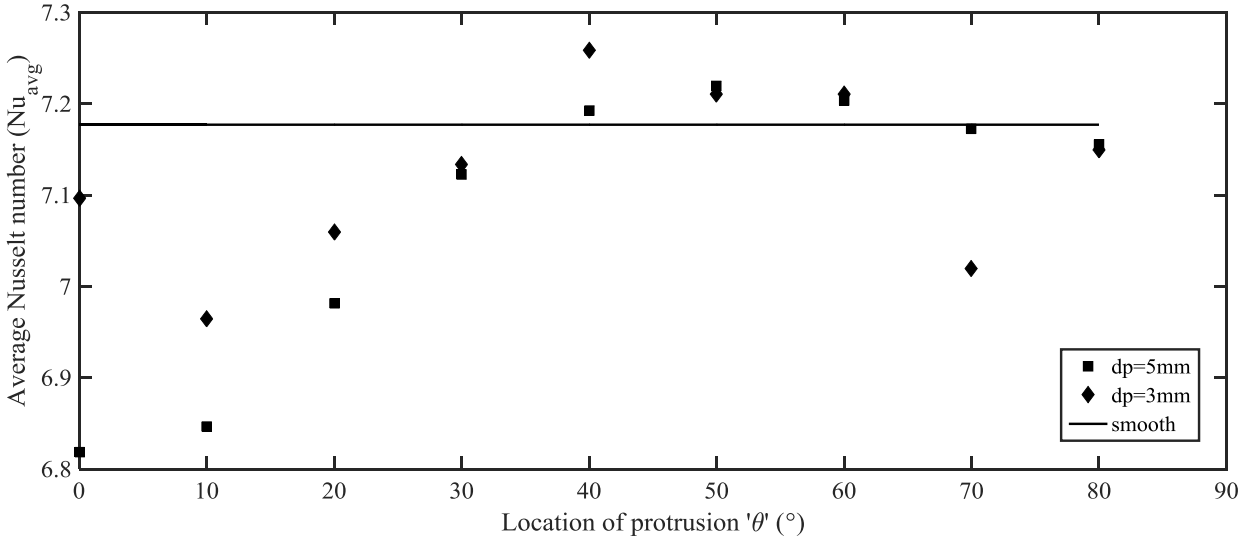

(a) Average Nusselt number

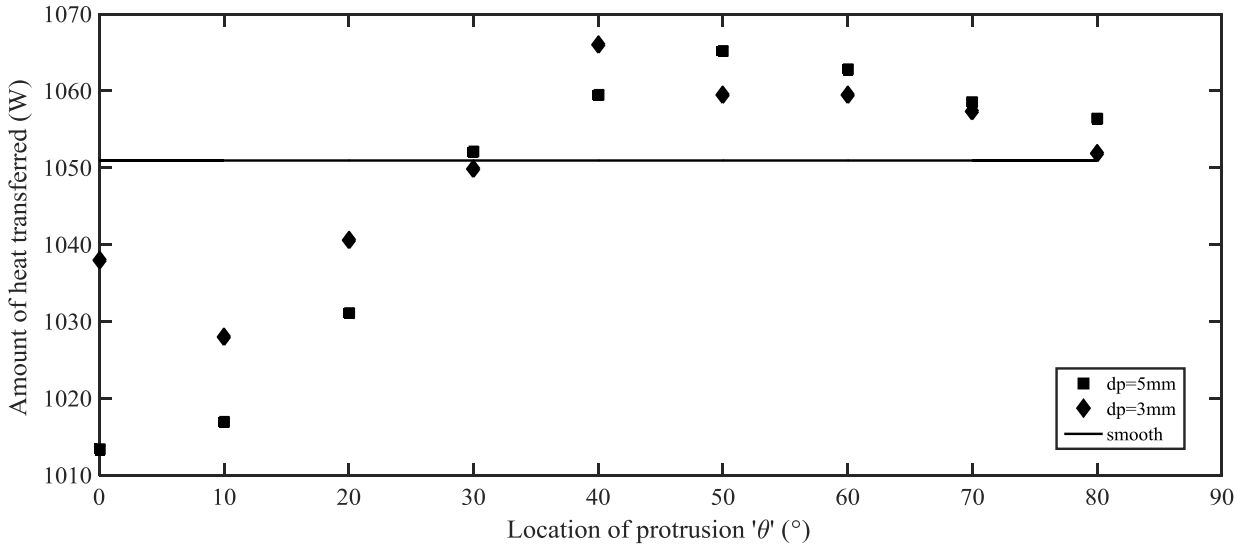

(b) Amount of heat transferred

Fig. 5. The effect of the location of the single protrusion for D=160mm, H/d=3 at Re=4060 on the heat transfer from the geometry. The flat lines in both the figures represent the performance of a smooth concave surface, as indicated in the legend.

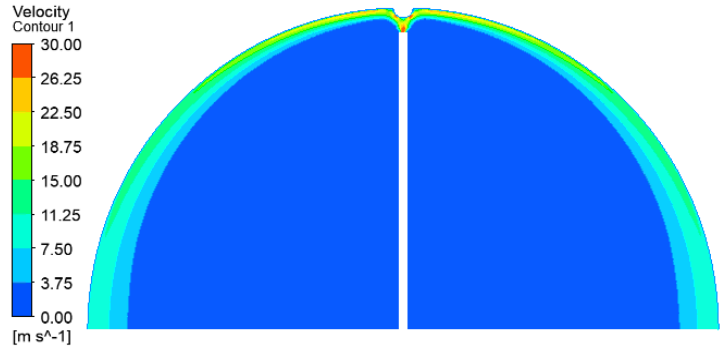

(a) $\theta = 0^0$

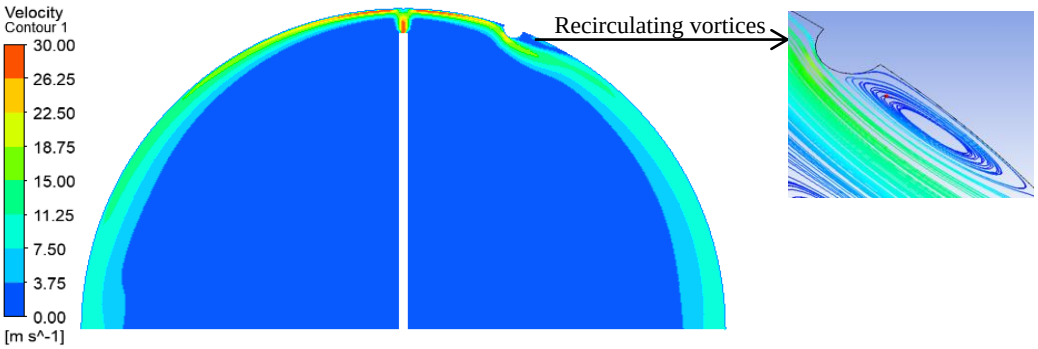

(b) $\theta = 20^0$

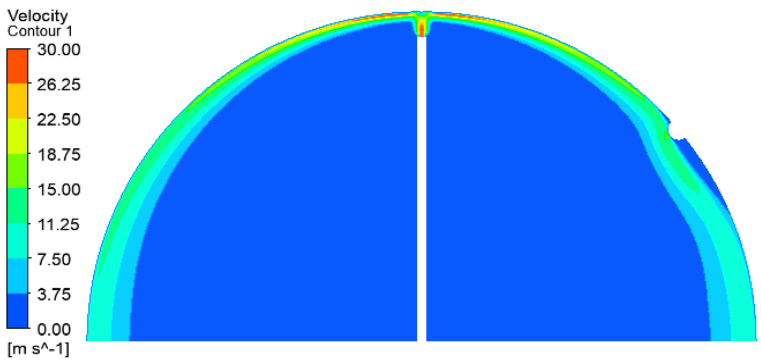

(c) $\theta = 50^0$

Fig. 6. Velocity contours corresponding to D=160mm and H/d=3 at Re=4060. Recirculating vortices are shown in the set of fig. 6(b).

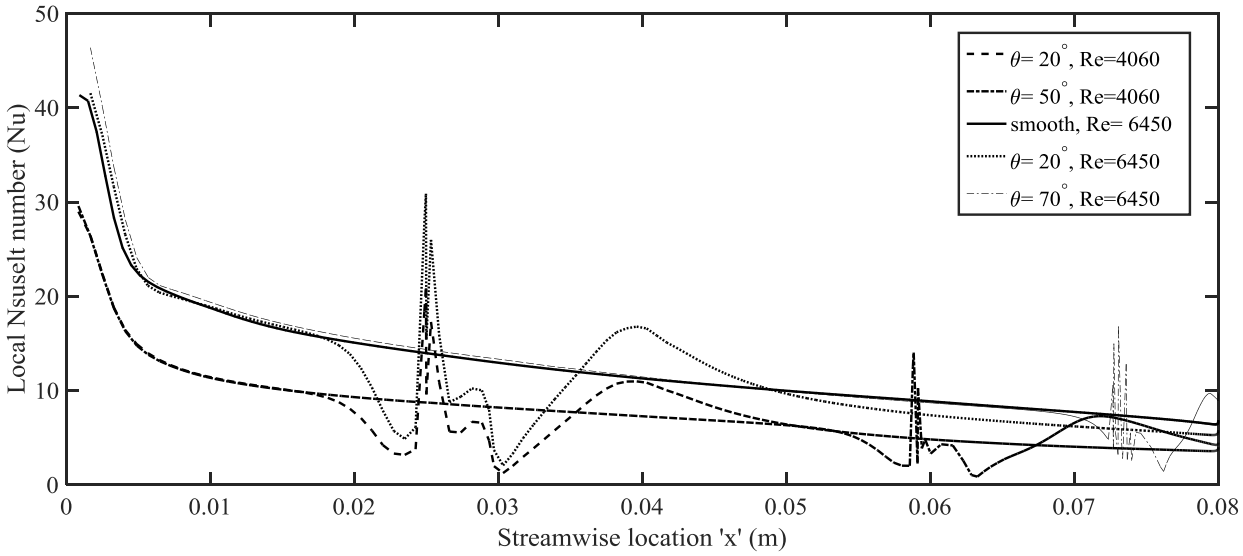

Fig. 7. Variation of the local Nusselt number at various location of protrusion for different combinations of Reynolds number. Results for the smooth surface at Re = 6450 are also shown to facilitate comparisons with a baseline case.

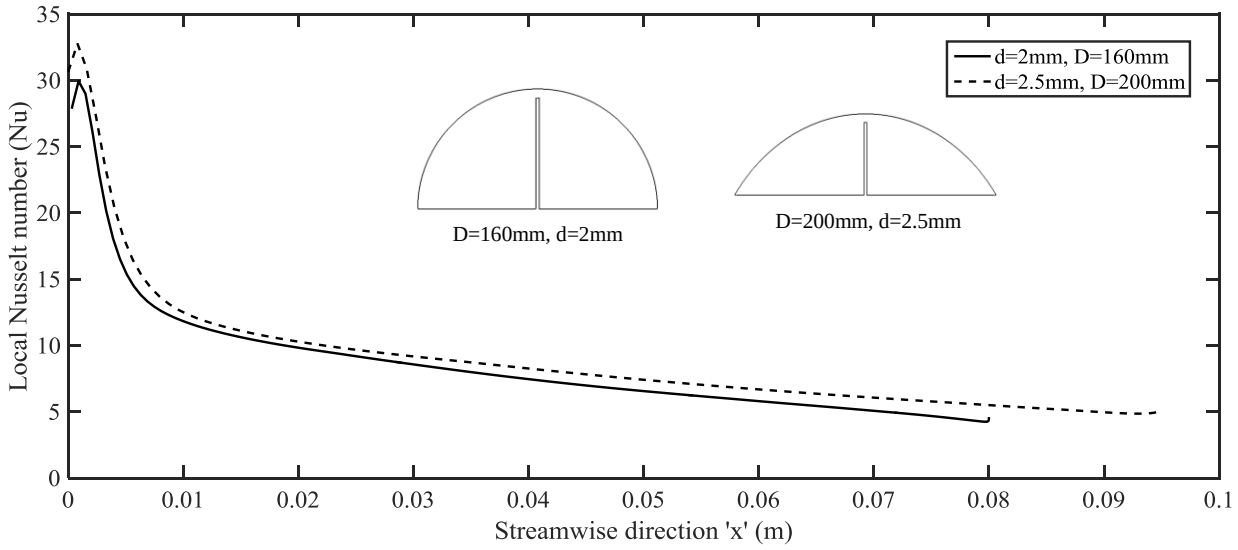

Fig. 8. Variation of the local Nusselt number for fixed curvature ratio (d/D =0.0125) at H/d=3 and Re=4060

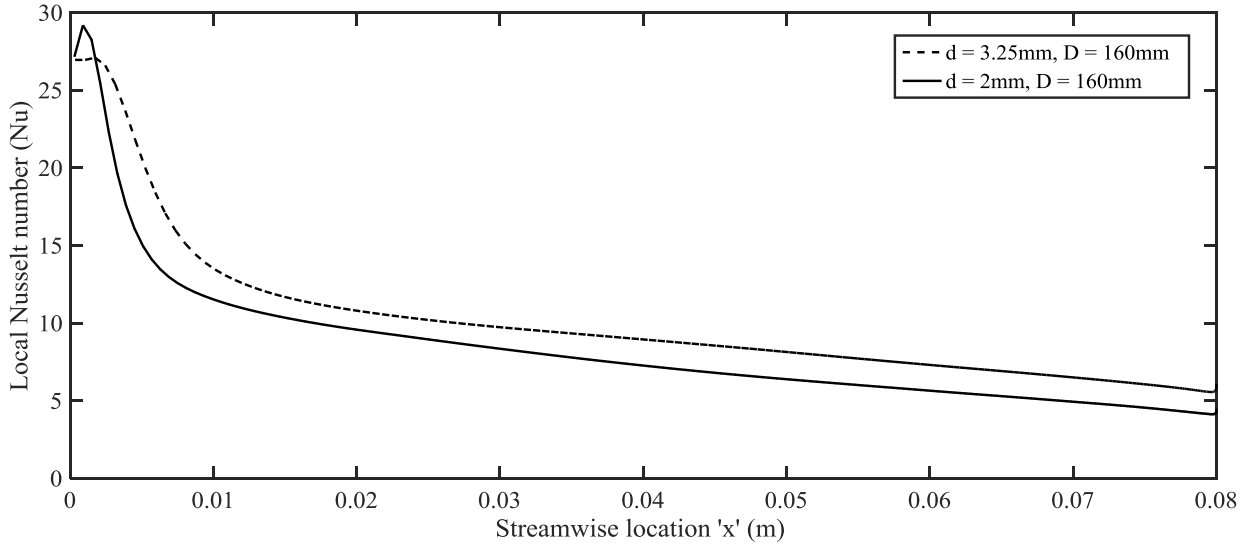

Fig. 9. Curvature effect on the local Nusselt number for a fixed diameter of concave surface (D=160mm, H/d=3, Re=4060)

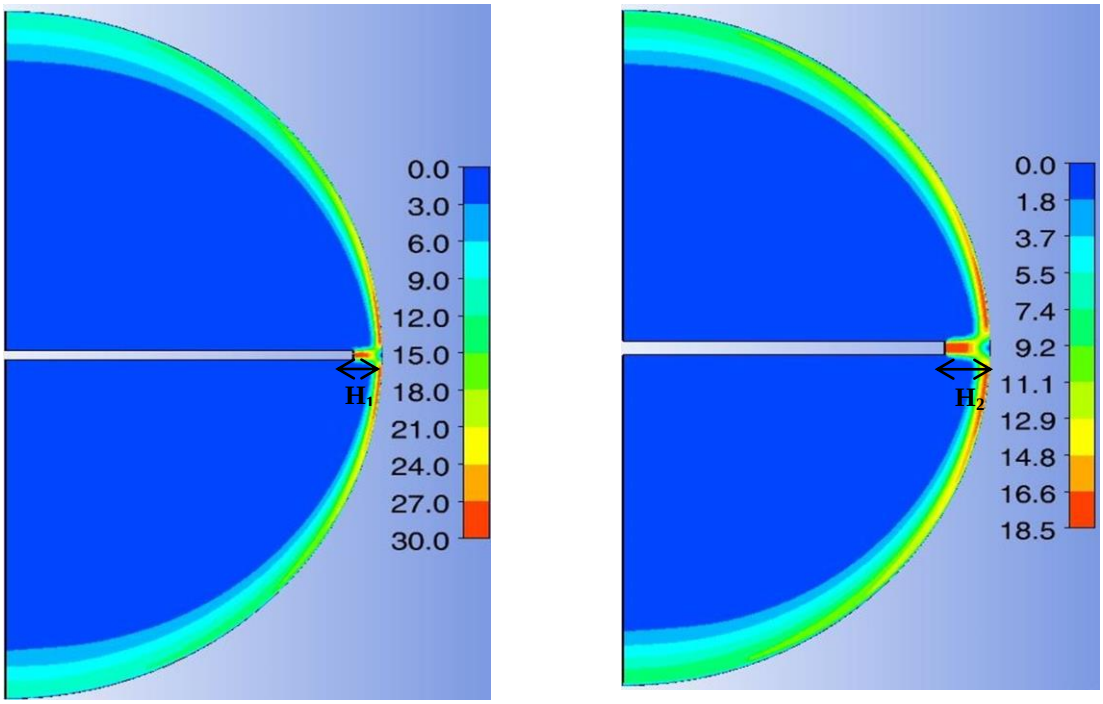

(a) d = 2mm **(b)** d = 3.25mm

Fig. 10. Curvature effect on the velocity contours at fixed diameter of concave surface (D=160mm, H/d=3, Re= 4060)

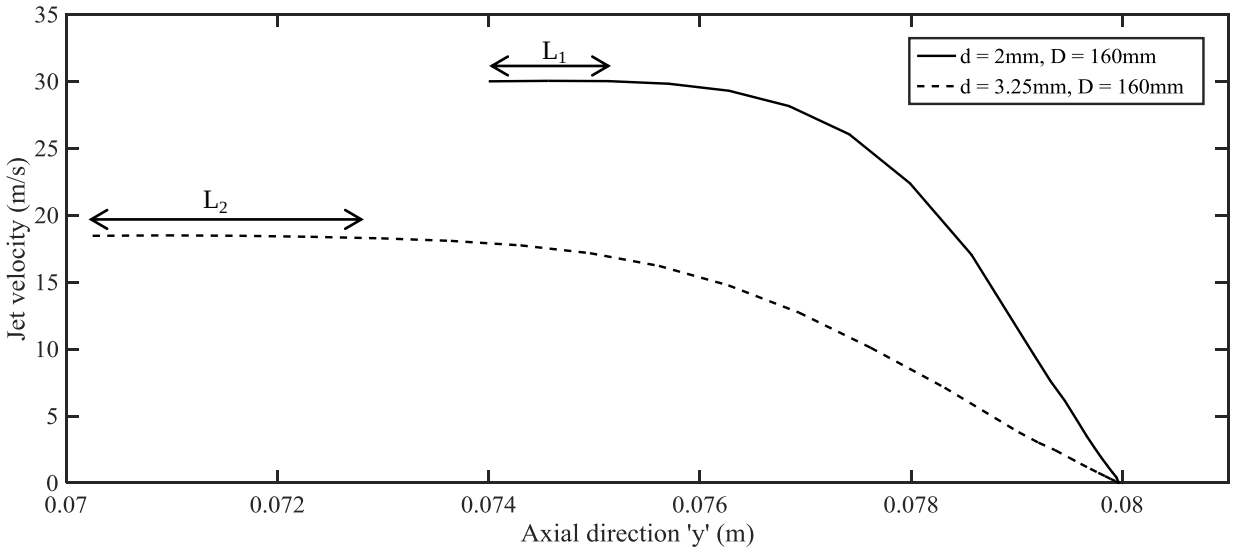

Fig. 11. Velocity of jet along axial direction at fixed diameter of concave surface (D=160mm, H/d=3, Re=4060)

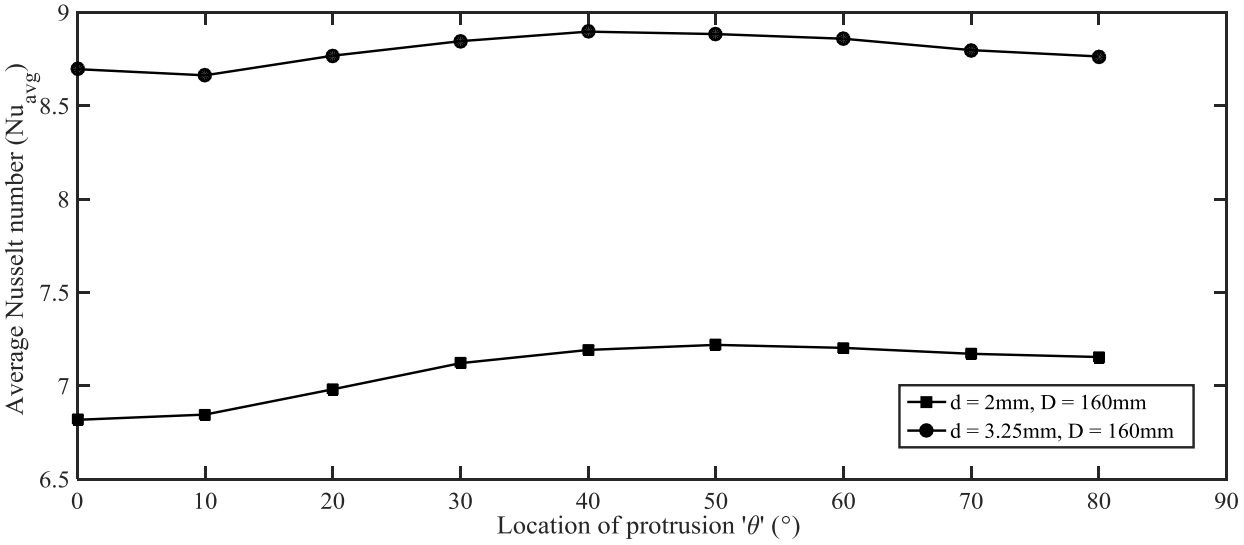

(a) Average Nusselt number

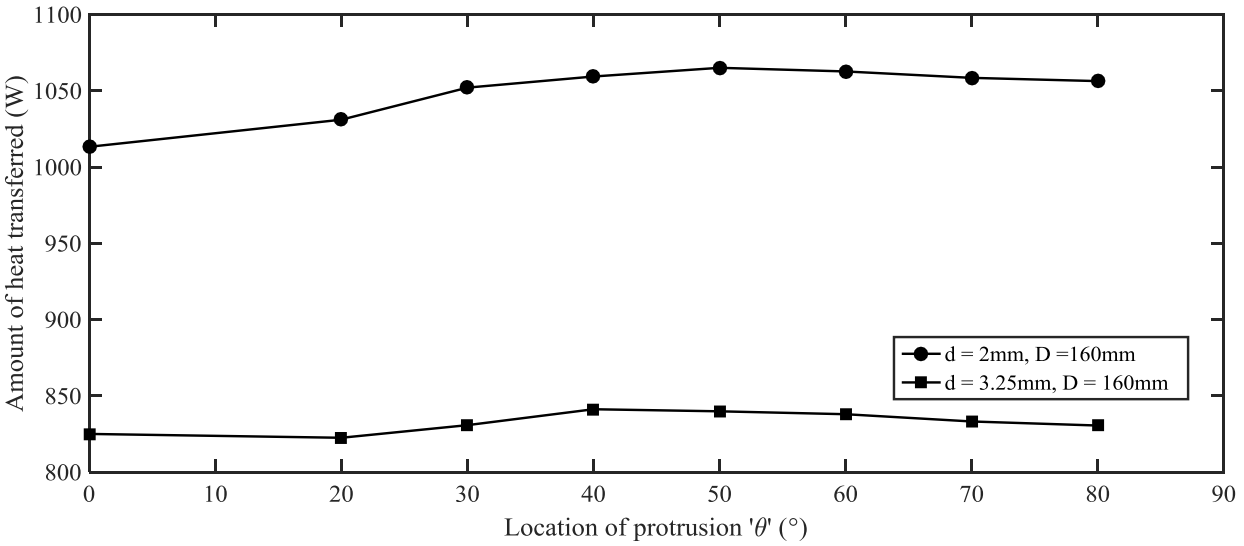

(b) Amount of heat transferred

Fig. 12. Curvature effect at fixed diameter of concave surface (D=160mm, H/d=3, Re=4060) on the heat transfer performance

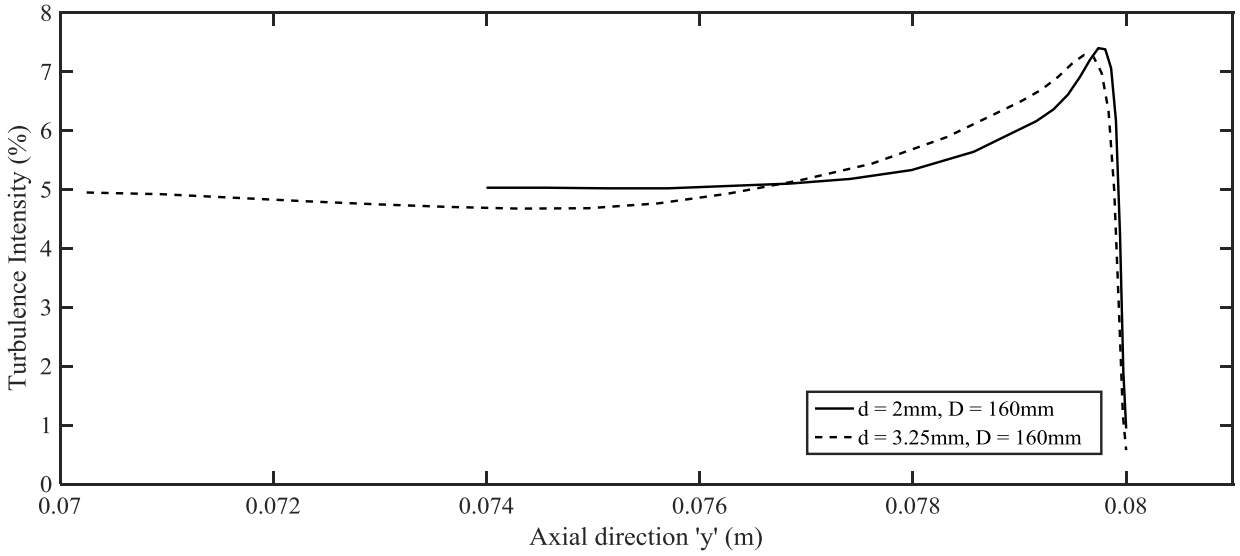

(a) Turbulence intensity behavior of jet along its axial direction

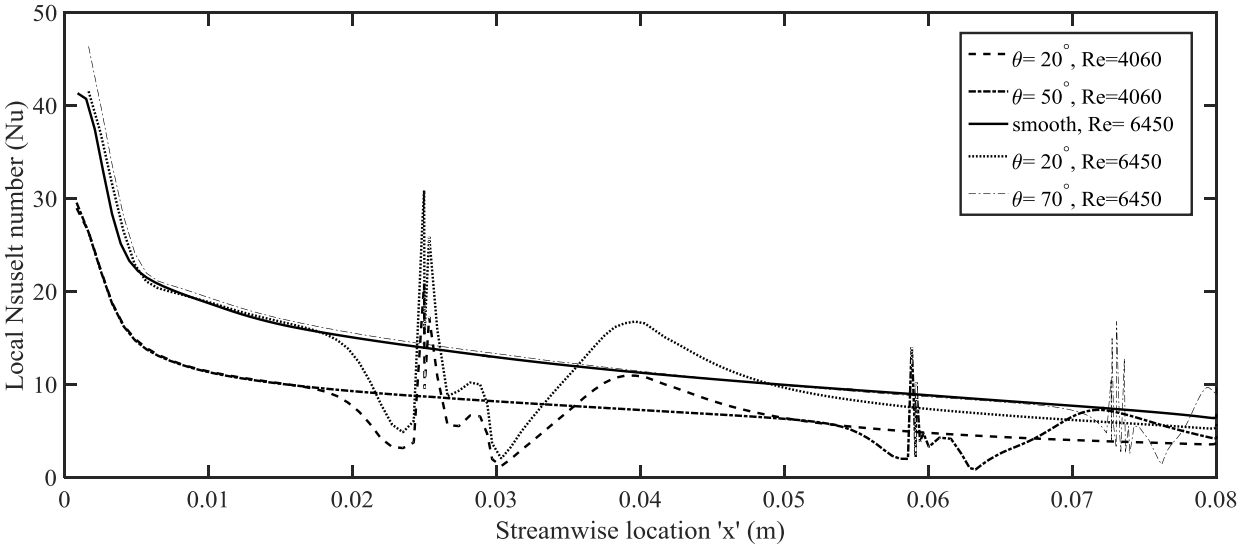

(b) Variation of the local Nusselt number along streamwise direction

Fig. 13. Turbulence intensity and local Nusselt number behavior for fixed diameter of concave surface (D=160mm, H/d=3, Re=4060)

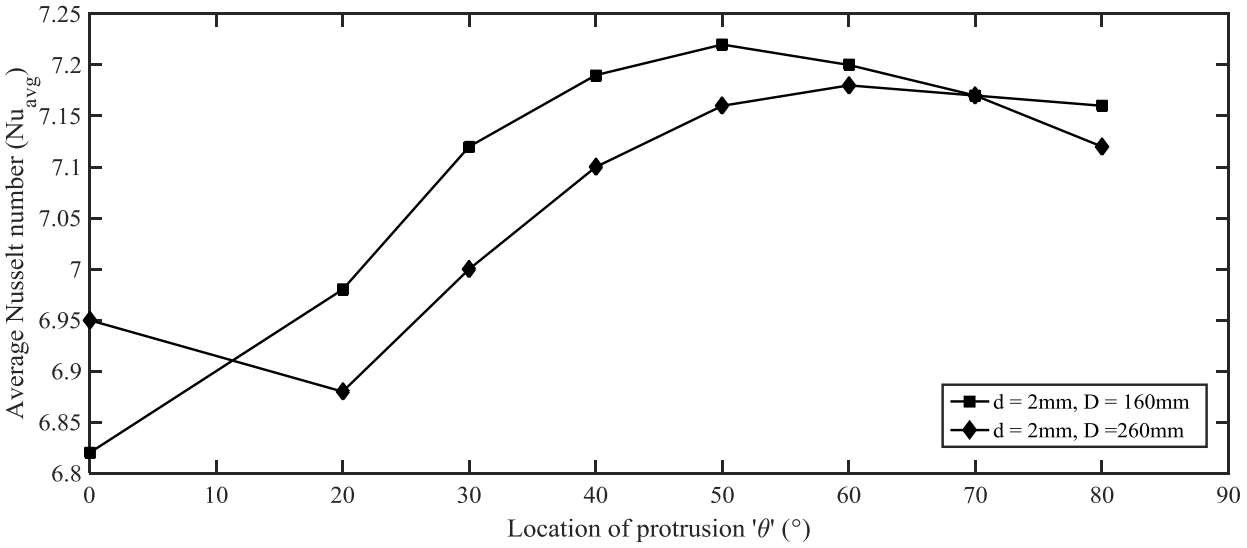

(a) Average Nusselt number

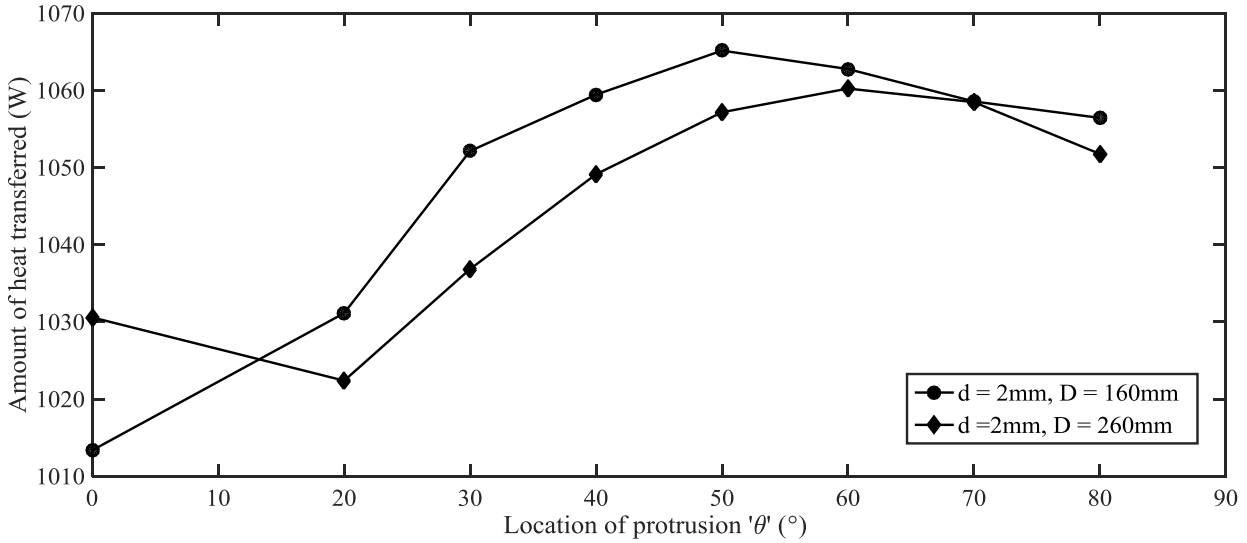

(b) Amount of heat transferred

Fig. 14. Curvature effect on the heat transfer performance at a fixed diameter of jet (d=2mm, H/d=3, Re=4060) for (i) D=160mm and (ii) D=260mm

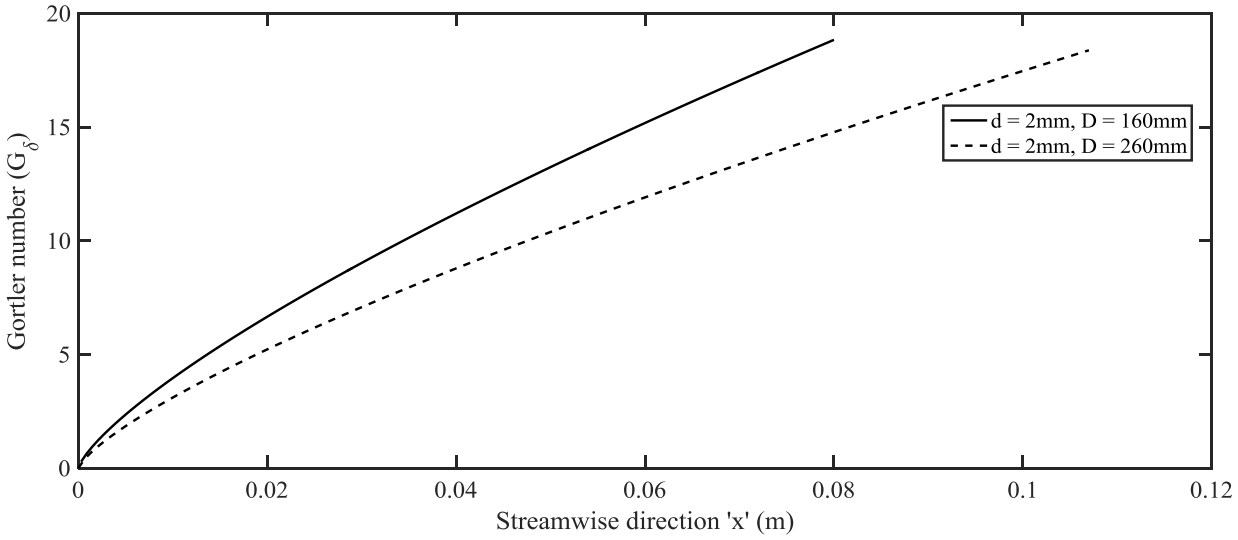

Fig. 15. Variation of Görtler number along the streamwise direction for two cases (i) d=2mm, D=160mm and (ii) d=2mm, D=260mm

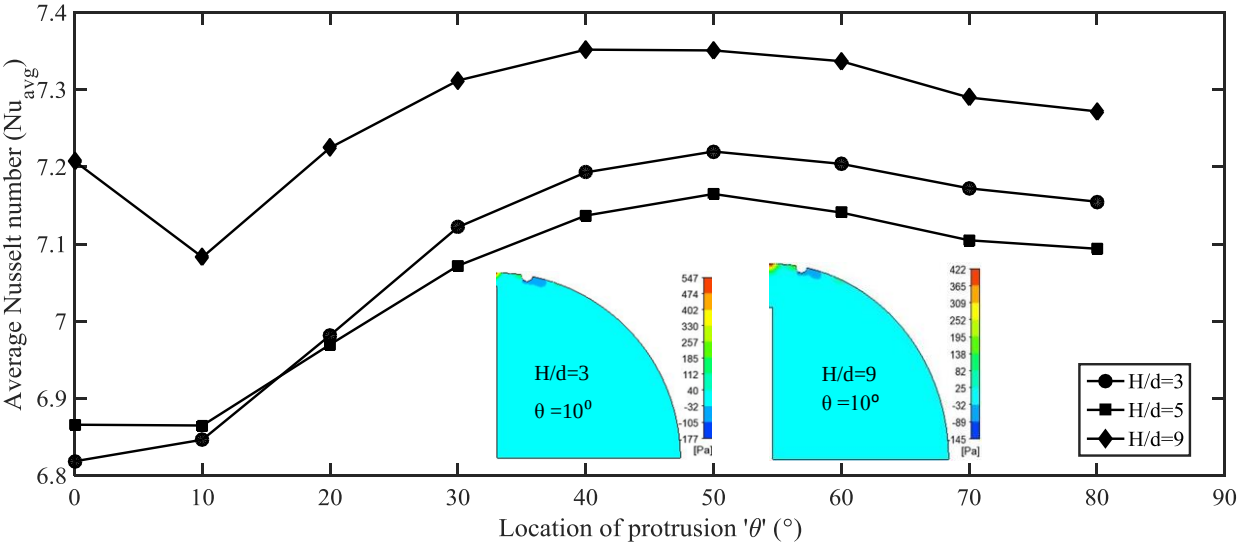

(a) Average Nusselt number and pressure contours

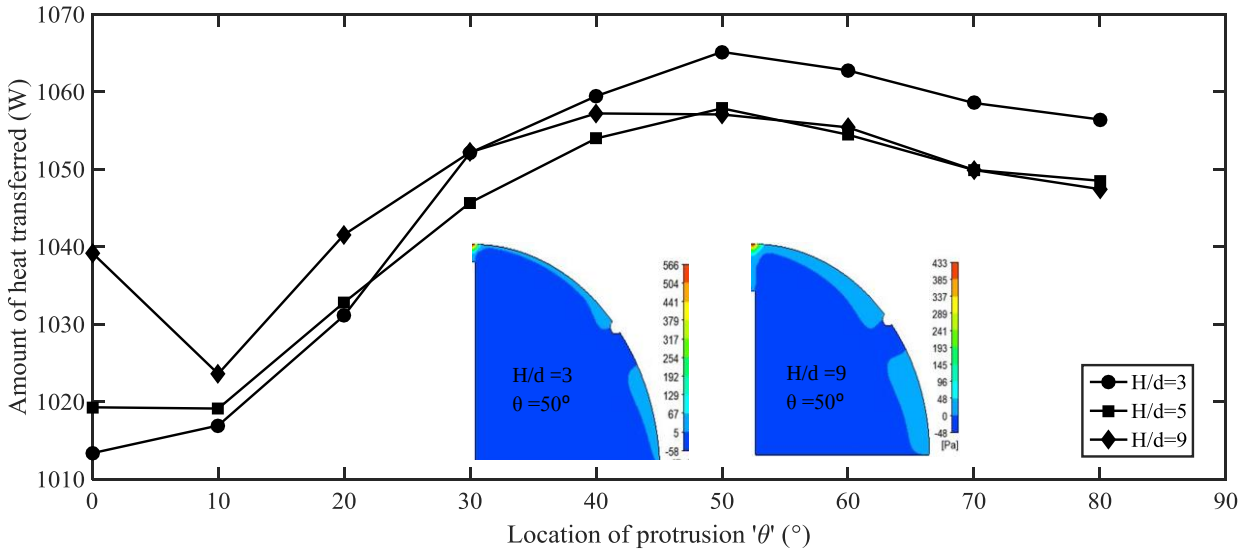

(b) Amount of heat transferred and pressure contours

Fig. 16. Effect of gap ratio on the heat transfer from the protruded concave surface (D=160mm, d=2mm, Re=4060)

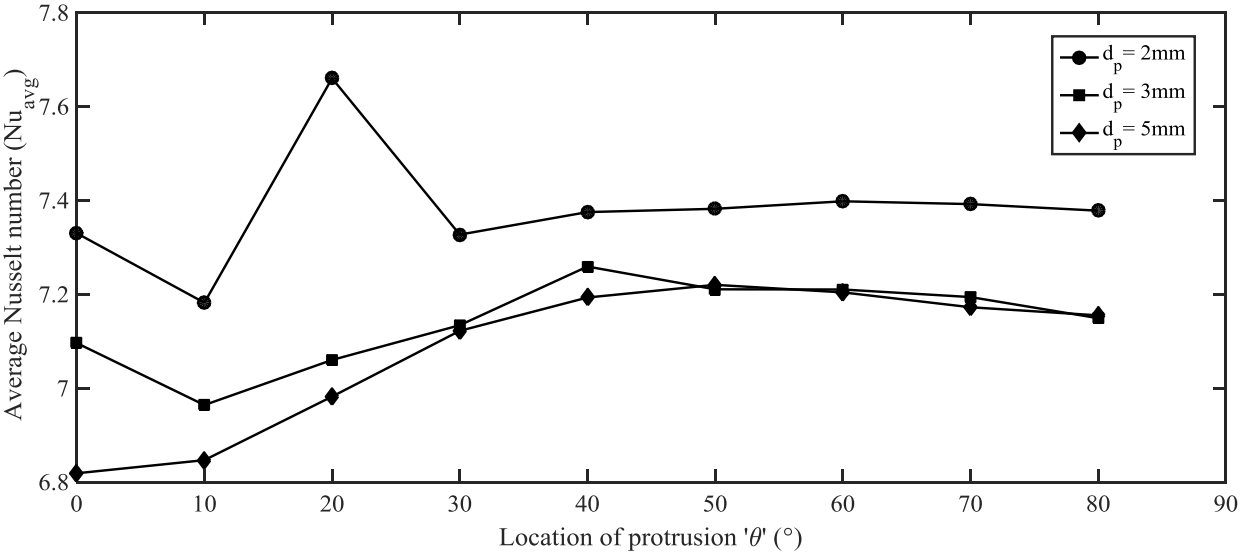

(a) Average Nusselt number

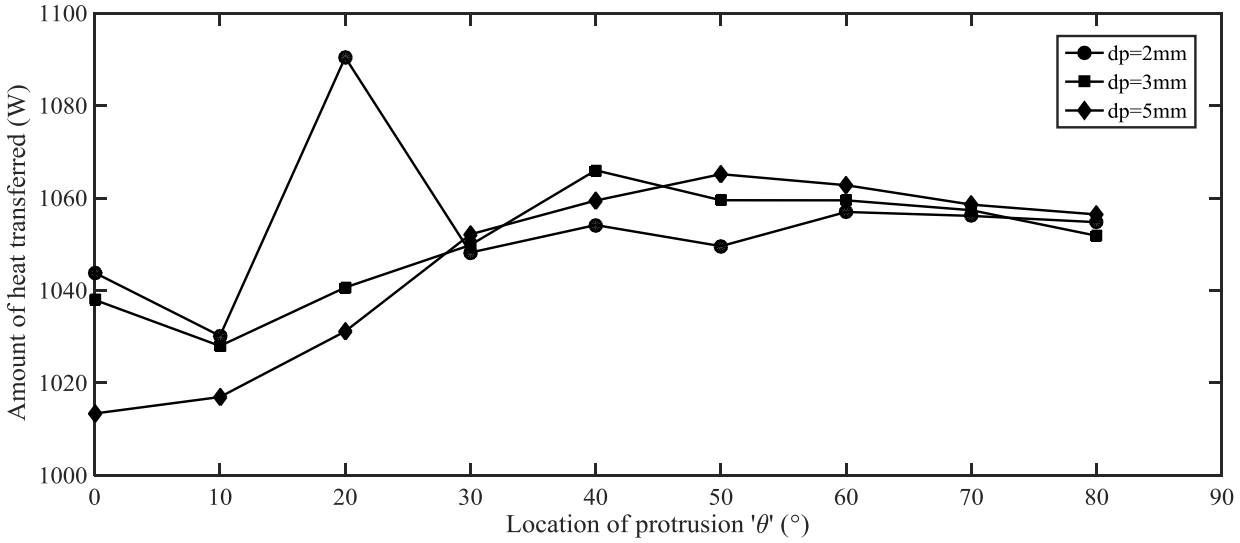

(b) Amount of heat transferred

Fig. 17. Effect of diameter of the protrusion on the heat transfer from the protruded surface

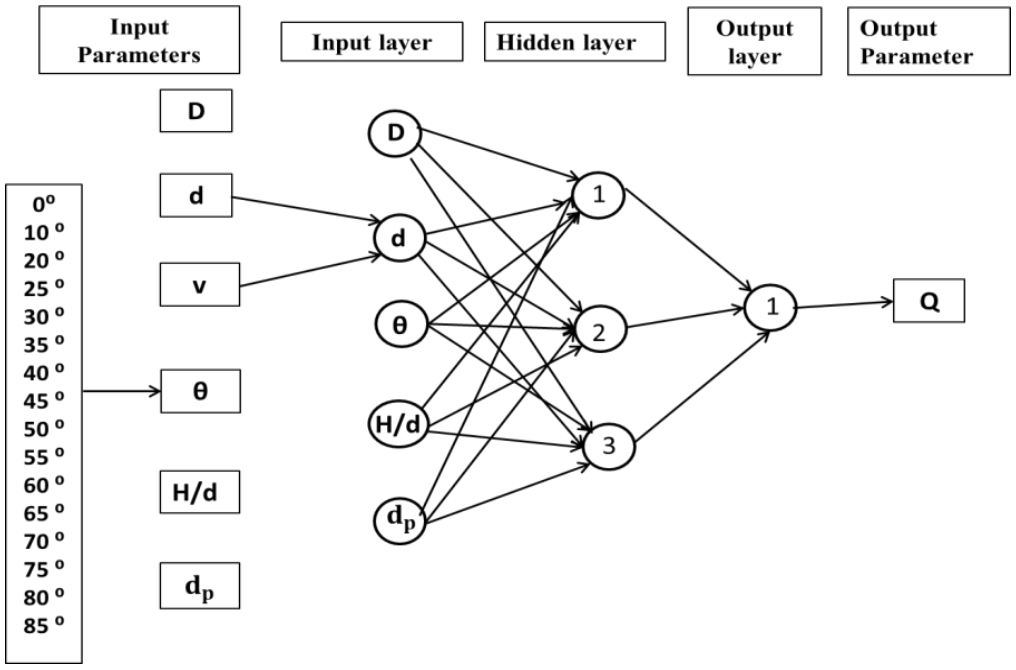

Fig. 18. Architecture of the ANN used in the present study

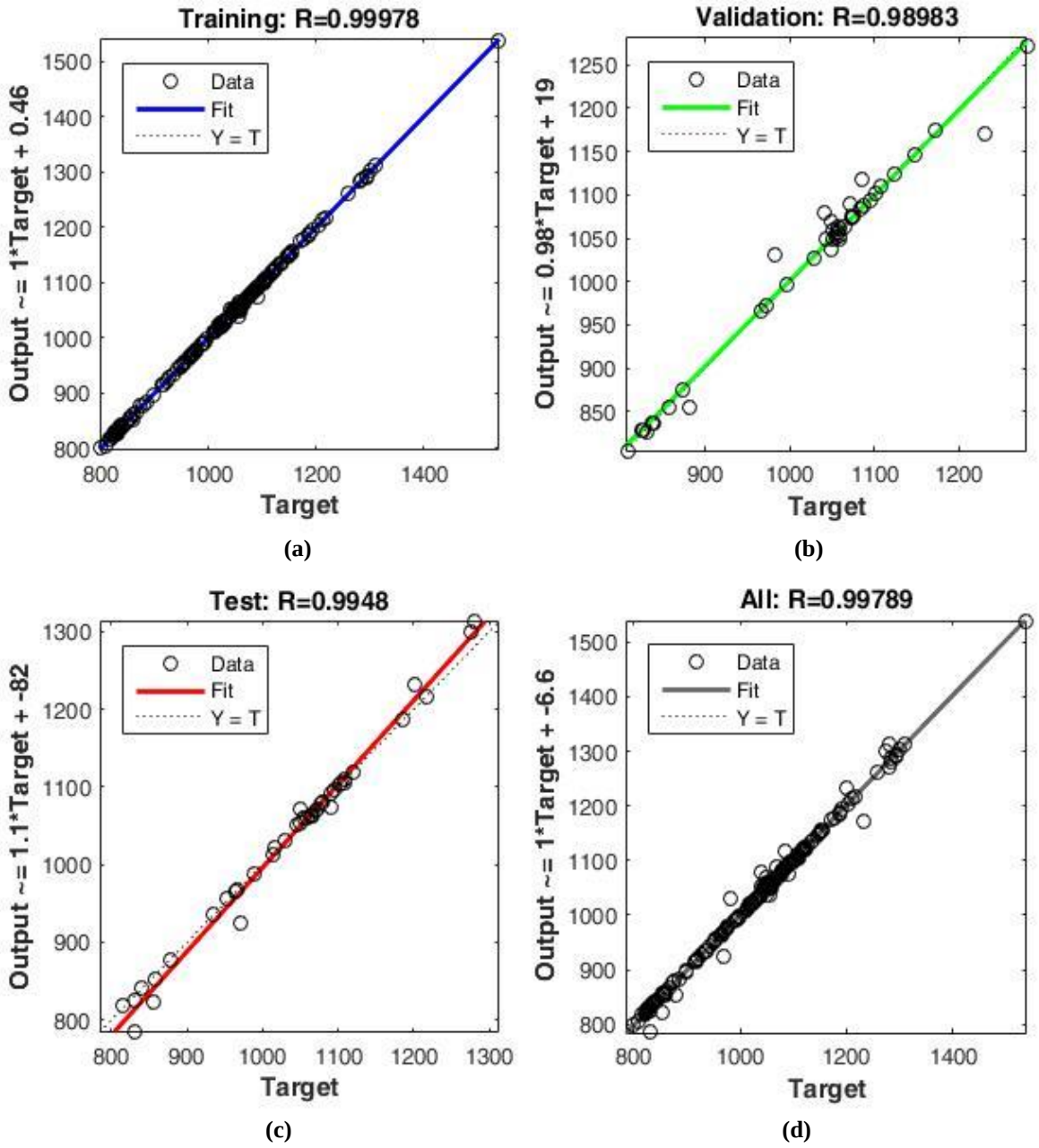

Fig. 19. Performance of the ANN in (a) training data set, (b) validation data set, (c) and (d) training, testing and validation data sets taken together

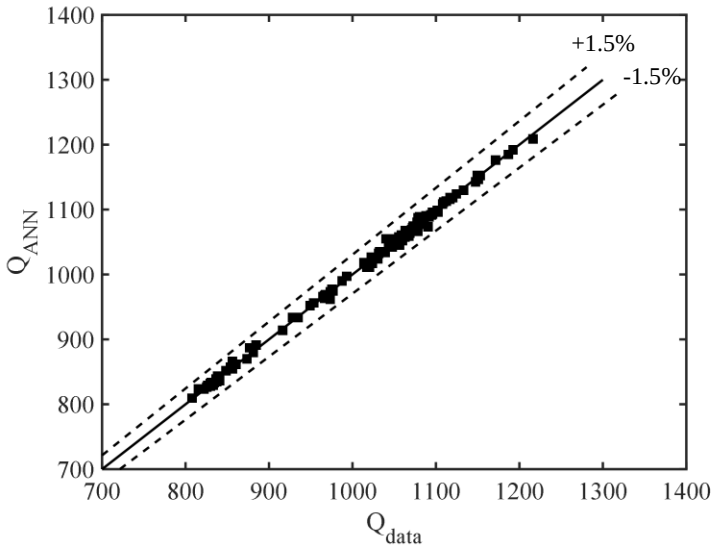

Fig. 20: Parity plot showing a comparison of Q_{data} and Q_{ANN} for data not used in training the network